Investigations on RSW Process Parameters for Tensile Strength and Nugget Quality of SS316L Sheet Joints- A Taguchi Approach

Sachin K. Dahake[1], Nilesh Diwakar[2], Shyamkumar D. Kalpande[3]

[1]Research Scholar, Department of Mechanical Engineering, RKDFIST SRK University, Bhopal, India. sachindahake@gmail.com
[2]Professor, Department of Mechanical Engineering, RKDFIST SRK University, Bhopal, India.
[3]Professor, Department of Mechanical Engineering, MET's IOE, Nashik, India.

The manuscript explores a detailed experimental design approach, integrating the Design of experiments (DoE) framework with optimization techniques to examine the spot weld strength and nugget formation in AISI 316L stainless steel sheets. The research utilizes tensile shear testing, macrostructure and microstructural analysis using an inverted microscope, to evaluate nugget formations and zones of joints. Taguchi method is successfully employed, with a signal-to-noise (S/N) ratio analysis to determine the effects of key parameters such as welding pressure, welding current, and weld time on the nugget diameter and tensile shear strength of spot welds. Results indicate that welding current significantly influences weld strength, also, the study provides an in-depth analysis of welding parameters' impact on nugget diameter, tensile-shear strength, and microstructure, including the fusion and heat-affected zones. Microstructural examination offers critical insights into the relationship between weld characteristics and welding parameters, suggesting optimal welding conditions. Taguchi analysis identifies the optimal welding parameters as a welding current of 10 kA, electrode force of 2 bar, and a weld time of 4 cycles, achieving maximum tensile shear strength.

Keywords: Resistance spot welding, Microstructure, Tensile strength, Taguchi method, Nugget diameter.

1. Introduction

Resistance spot welding (RSW) is a widely used technique for joining metallic sheets due to its high efficiency and cost-effectiveness in industries such as automotive, aerospace, and manufacturing [1−4]. AISI 316L stainless steel, known for its exceptional corrosion resistance and mechanical strength, is frequently used in critical applications [2, 5−6]. The mechanical

properties of RSW joints in AISI 316L steel are influenced by several process parameters, including welding current, welding time, pressure, and electrode shape [6−8]. Although RSW is prevalent across various sectors, there is still a substantial need for comprehensive studies to thoroughly understand how these parameters impact the mechanical properties of AISI 316L joints [9−11]. While previous research has explored the effects of process parameters on the mechanical characteristics of welded joints in various materials [12−14], a detailed investigation specific to AISI 316L steel joints is crucial [15]. Optimizing the process parameters for RSW of AISI 316L joints is essential to achieving the desired mechanical qualities such as tensile shear strength, hardness, and fatigue behavior [16−18]. Additionally, a deeper understanding of the microstructural changes caused by different welding conditions is critical for enhancing the mechanical effectiveness of these joints [19−21]. Given the broad range of applications for AISI 316L, particularly in environments prone to corrosion like maritime and chemical processing, it is vital to investigate the impact of welding conditions on its corrosion resistance comprehensively [2, 22, 23]. Examining the relationship between process parameters, microstructure, mechanical properties, and corrosion resistance of RSW joints in AISI 316L steel will contribute significantly to improving the welding process for diverse industrial applications [24−26]. This study aims to address the current research gap by conducting a thorough investigation of how process parameters affect the mechanical properties, microstructure, and corrosion resistance of RSW joints in AISI 316L steel. Through extensive testing and analysis, this research seeks to optimize welding conditions to produce strong and durable joints, thereby addressing the need for a deeper understanding of this critical aspect of welding technology. The influence of welding current and electrode force on microstructure formation in the nugget zone and the resulting failure patterns in RSW joints are key factors that affect the overall mechanical characteristics and performance of these joints.

Welding current directly impacts the heat generated during the RSW process [5]. Increased welding currents lead to greater heat input, which influences the development of the weld nugget. Higher temperatures can result in grain growth and coarsening within the nugget area [14, 15]. Variations in welding current affect the grain size and morphology within the nugget zone, where increased thermal energy might lead to larger grain formation, potentially impacting mechanical properties such as hardness and tensile shear strength [6, 27]. Excessive welding current can lead to the formation of large grains and unwanted phases, causing brittleness and vulnerability to cracking in the nugget or heat-affected zone (HAZ) [6, 28]. This can result in premature failure under mechanical or thermal stress. Liquid metal embrittlement (LME) is another phenomenon where elevated welding currents can induce embrittlement and eventual failure, especially in dissimilar material joints. This occurs when the liquid phase generated at higher temperatures diffuses into the base material, leading to embrittlement [14, 29]. The electrode force also plays a significant role, affecting the size and shape of the nugget by determining the contact area and pressure on the materials being welded [30]. Higher forces often result in larger nugget sizes as they promote more material deformation and higher heat concentration at the joint contact [7, 31]. Proper application of electrode force ensures even distribution of pressure along the joint contact, resulting in a uniform microstructure within the nugget zone [1, 32]. Inadequate electrode force can lead to incomplete fusion or insufficient penetration at the interface, resulting in weak or intermittent bonding and eventual joint failure [9, 33]. Insufficient electrode force may also result in

inadequate nugget formation or weak bonding between sheets, leading to failure through nugget pullout or shear mechanisms under load [10, 34]. Balancing the welding current and electrode force is crucial for achieving favorable microstructures and minimizing failures in RSW joints. This balance is essential to ensure the appropriate heat input for creating a robust nugget while avoiding adverse effects such as grain enlargement, brittleness, or inadequate bonding. A methodical understanding and management of these aspects are vital for producing strong and reliable RSW connections in AISI 316L steel, thereby enhancing their mechanical properties and overall effectiveness. Investigating RSW process parameters for SS316L sheet joints is essential for optimizing tensile shear strength and nugget quality. SS316L is widely used in critical applications that demand high performance.

Understanding these parameters ensures consistent joint quality, improves mechanical properties, and reduces defects, leading to cost savings. The Taguchi approach offers a systematic and efficient method for identifying optimal conditions with fewer experiments, ensuring robust and repeatable results. The material used in this study is 316L stainless steel, renowned for its excellent corrosion resistance and widespread use in pharmaceuticals, petrochemicals, and food processing industries. Welding of 316L is challenging due to its heat sensitivity, which can lead to distortion and undesirable microstructures. RSW is chosen for its ability to provide localized heating and minimize thermal distortion. Despite extensive research on 316L welding, optimizing parameters and understanding microstructural changes remain areas of concern. This investigation aims to improve the weld quality, mechanical properties, and reliability of 316L stainless steel welds.

2. Materials and Method

The chemical composition of AISI 316L, utilized for the current experiments, is presented in Table 1. The composition was determined using spectromaxx chemical composition testing machine.

Table 1: Chemical Composition of 316L stainless steel

Grade	C%	Mn%	P%	S%	Si%	Cr%	Ni%	Mo%
316L	0.022	1.25	0.045	0.004	0.42	16.16	10.03	2.06

Types 316 and 316L are austenitic stainless steels that contain molybdenum. They offer greater resistance to general corrosion and pitting/crevice corrosion compared to ordinary chromium nickel austenitic stainless steel, like type 304. Additionally, these alloys have superior resistance to deformation under constant load, increased resistance to fracture under stress, and enhanced ability to withstand stretching forces at high temperatures. Types 316 and 316L often have a molybdenum content of 2 to 3% to enhance their corrosion resistance. Furthermore, it possesses exceptional corrosion resistance and exhibits high levels of strength. Both types 316 and 316L alloys exhibit exceptional weld ability and formability, characteristic of austenitic stainless steels. Stainless steel 316L exhibits superior properties in terms of creep resistance, stress rupture resistance, and tensile shear strength at high temperatures when compared to chromium-nickel austenite stainless steel.

2.1 Taguchi method for experimentation

The analysis is carried out using a Taguchi technique which is a robust design of experiments

strategy, to examine the impact of process parameters on the tensile shear strength of AISI 316L welded joints. The variables considered included welding current (measured in kilo-amperes, kA), pressure (measured in bars), and weld time (measured in cycles). Each factor was evaluated at three specific levels: 6, 8, and 10 for welding current; 2, 4, and 6 for pressure; and 4, 6, and 8 for weld duration. Welding trials were performed on AISI 316L steel samples using various combinations of these parameters according to the Taguchi L9 orthogonal array. The tensile shear strength of each welded junction was measured and recorded in MPa, providing critical data for analysis. Taguchi technique was fully utilized to determine the Signal-to-Noise (S/N) Ratio for every combination of welding parameters. The average tensile shear strength values for each parameter setting were calculated to assess the effectiveness of different combinations. The recorded tensile shear strength readings from the welding trials were compiled and organized for every possible combination of welding settings. The analysis of the S/N ratio and mean was conducted to identify the most effective parameter configurations for maximizing the tensile shear strength of AISI 316L welded joints.

2.2 Preparation of the specimen

For the specimen preparation, a 0.4 mm thick metal sheet made of SS 316L was used. Each specimen was prepared with dimensions of 100 mm x 25 mm, utilizing wire cut Electrical Discharge Machining (EDM) for precise fabrication. Two sheet specimens of 100 mm x 25 mm (length x width) were then joined together using a lap joint configuration, adhering to the AWS C1.1M/C1.1:2012 standard, as illustrated in Figure 1.

Figure 1(a, b): (a, b) Details of sample preparation
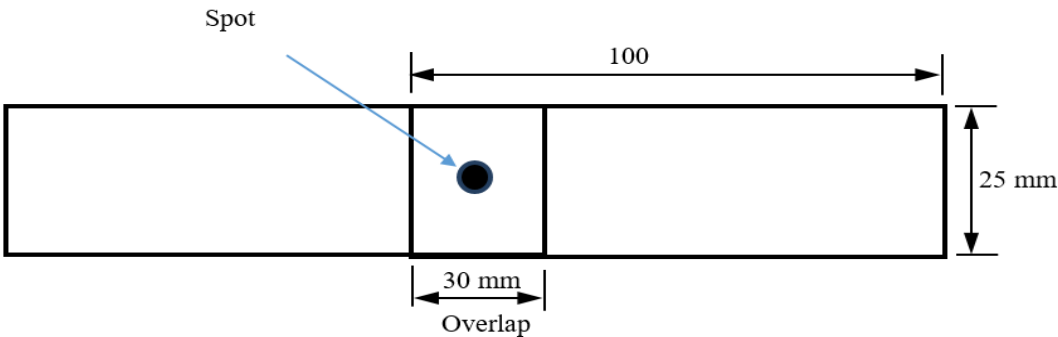
Figure 1(a): Layout of sample preparation

Figure 1(b): Photograph of tensile shear strength specimen

3. Experimentation

Experiments were conducted using electrical resistance spot-welding, regulated by both current and time, with a capacity of 120 kVA machine, employing a pneumatic application mechanism. The experimental setup is shown in Figure 2, while Figure 3 illustrates the machine's control panel. Based on trial experiments, the levels of welding current were set at 6, 8, and 10 kA. Electrode force levels were selected at 2, 4, and 6 bars, and the duration of the welding process was considered at 4, 6, and 8 cycles. Throughout all experiments, the squeeze time was kept constant at 35 seconds. In this setup, the sheets were joined through electrical resistance spot welding, with careful adjustments made to parameters like electrode force, welding current, cycle time, and the diameter of the fixing electrode. The experiments were conducted by measuring the responses, specifically the tensile shear strength of the welds. Minitab software was then used for data analysis, where the S/N ratio was calculated using a specific equation aimed at maximizing the "better" characteristics The S/N ratio was calculated using following equation for maximum the better characteristics. Table 2 shows the detailed plan of experimentation with measured responses.

$$\left(S/N \right) = -10 \log \left(1 \middle/ \frac{1}{n} \sum_{i}^{n} y_i^2 \right)$$

(1)

Figure 2: Photograph of RSW machine used to make the joints
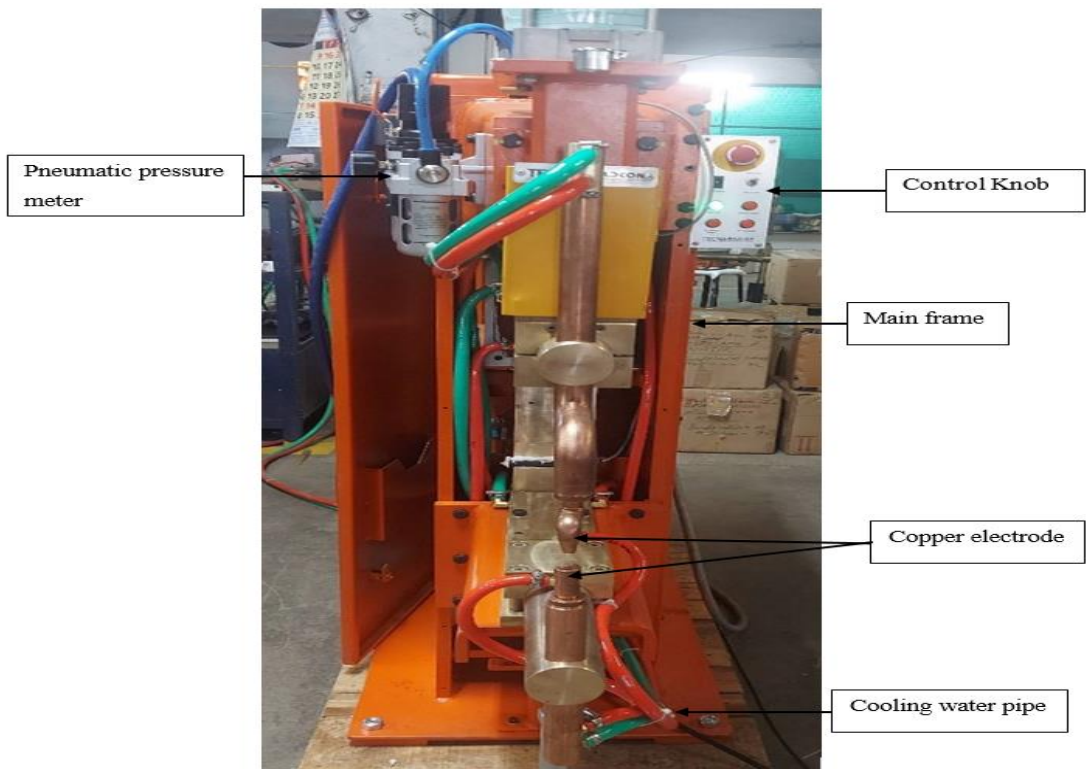
Figure 3: Digital display of control panel

3.2 L9 orthogonal array and testing results

Table 2: Plan of experiments with testing results

Sr. No.	Welding current (KA) – A	Pressure (Bar) - B	Weld time (Cycles) - C	Tensile shear strength (MPa)	S/N Ratio	Mean
1	6	2	4	272.12	48.69	272.12
2	6	4	6	199.21	45.98	199.21
3	6	6	8	131.82	42.39	131.82
4	8	2	6	231.05	47.27	231.05
5	8	4	8	269.40	48.60	269.40
6	8	6	4	248.90	47.92	248.90
7	10	2	8	254.20	48.10	254.20
8	10	4	4	271.64	48.67	271.64
9	10	6	6	285.12	49.10	285.12

Figure 4 are the specimens prepared after spot weld of above combination and marked with numbers.

Figure 4: Photograph of Specimens prepared
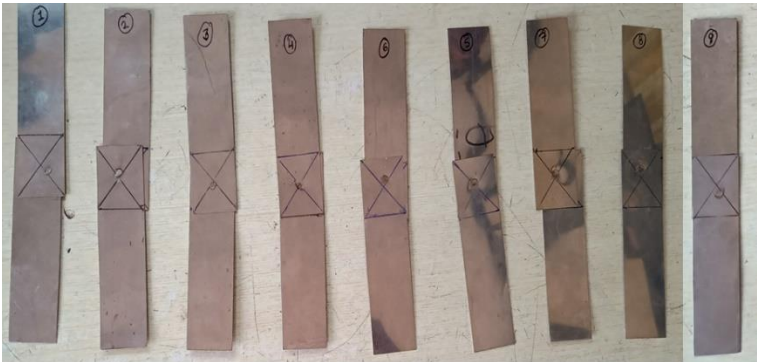
4. Results and discussion

4.1 Tensile shear strength: In the study, tensile shear strength testing was employed to evaluate the strength and properties of the welded joints. For specimens with a thickness of 0.4 mm or greater, the weld grips on the test machine is adjusted to address potential offset loading issues caused by the specimen's thickness. This adjustment is necessary to ensure accurate testing results. The tension shear test, chosen for its simplicity and cost-effectiveness, was utilized to assure production quality. For these tests, a Universal Testing Machine (UTM) with a capacity range of 0 to 40 tons, ensuring precise measurement of mechanical properties was utilised.

To determine the size of the weld nugget, the welded samples were sliced perpendicular to their direction of welding using a basic cutting machine. By employing metallurgical polishing techniques, samples were meticulously prepared and subsequently treated with a solution for etching. The weld zone was collected in an image analyzer utilizing the interface of a metallurgical microscope, as depicted in Figure 5.

4.2 Microstructural analysis: Microstructural analysis of welded joints involves macro-etch testing to examine the structure and properties of the material. For this small sample from the welded junction is removed from joint specimens at their intersection, and treating them with a mild acid blend specific to the material. For SS316L, a common etchant is a mixture of hydrochloric acid (HCL) and nitric acid (HNO3), known as aqua-regia is used. The process follows ASTM E407 standards for specimen preparation and etching. The acid etching technique provides a clear view of the interior composition of the weld, revealing the extent of penetration, and any indications of insufficient fusion, poor root penetration, internal porosity, or cracking at the fusion line.

The microstructure analysis reveals that a totally austenitic microstructure exhibits greater susceptibility to cracking compared to the microstructure that contains a minor proportion of ferrite. The microstructure of the AISI 316 L stainless steel base metals consists of austenitic polygonal grains with a low proportion of delta ferrite. The grain size is classified as ASTM 7. Delta ferrite exhibits elongated stringers in the rolling direction. The macrostructure of the nugget is shown in Figure 6. The region labeled "FZ" refers to the fusion zone, which is the area where the base metals have completely melted and solidified during the welding process. This zone typically exhibits a cast or solidified microstructure distinct from the base metal. The region labeled "BM" stands for base metal, which is the unaffected parent material away from the weld zone. The region labeled "HAZ" represents the heat affected zone. This is the area adjacent to the fusion zone that experienced elevated temperatures during welding, high enough to cause microstructural changes but not complete melting. The HAZ often exhibits a microstructure that is different from both the fusion zone and the base metal due to the thermal cycles experienced. In the image, the HAZ is clearly visible as a distinct region surrounding the fusion zone. The yellow circle highlights the fusion zone (FZ), where the complete melting and solidification occurred during welding.
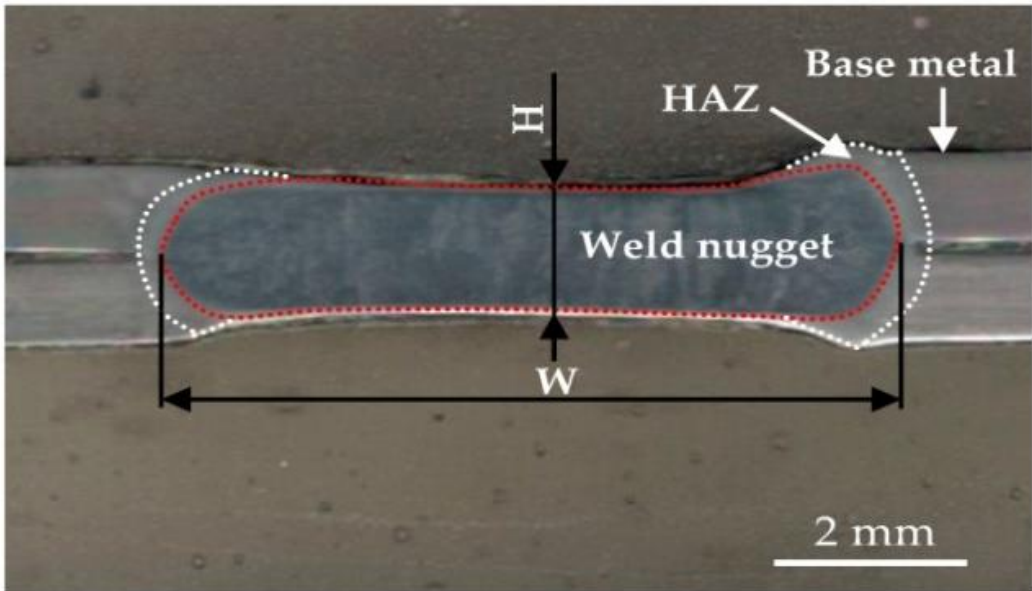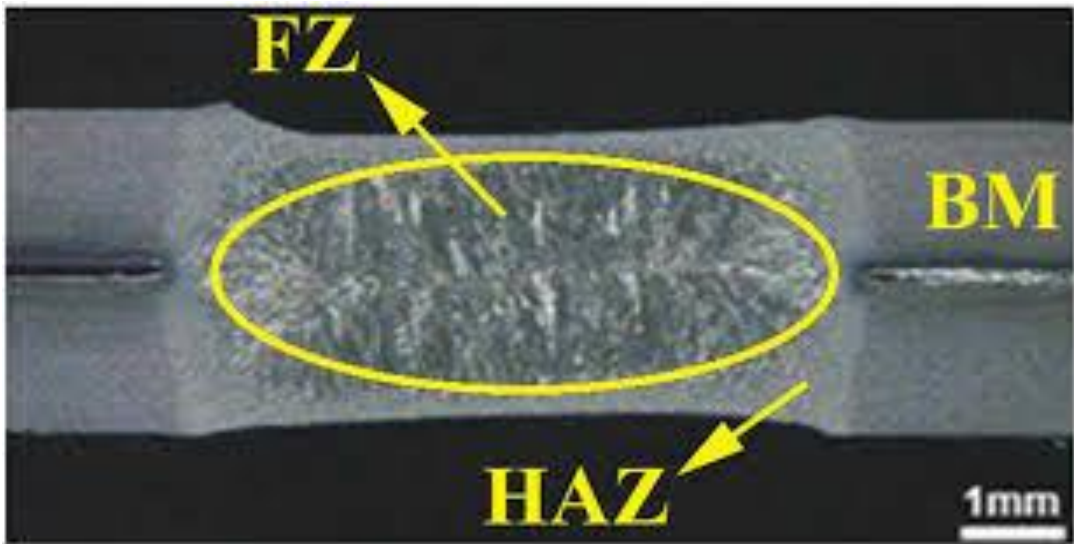
Figure 5: Macrostructure of welded joint

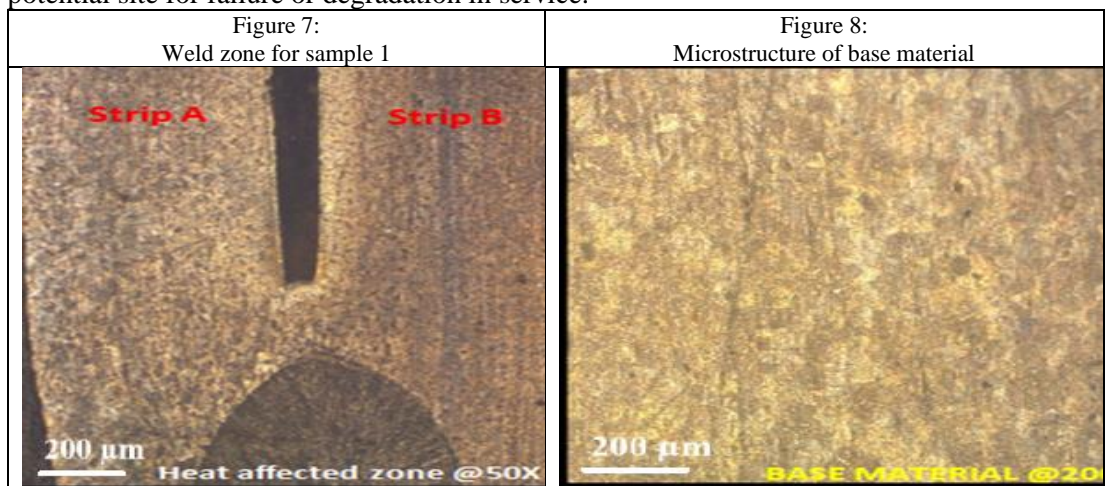Figure 6: Macrograph showing different regions in RSW joint of 316L steel

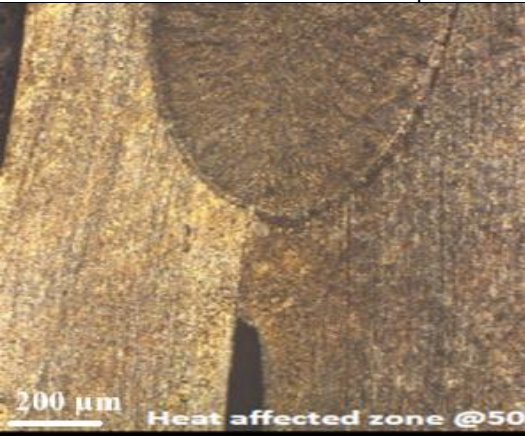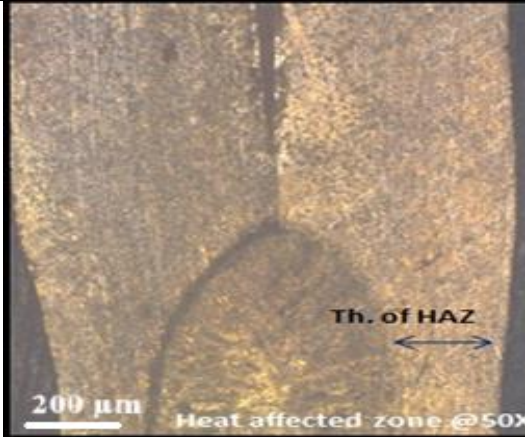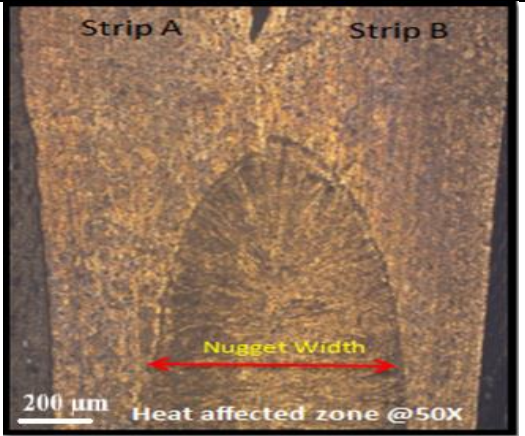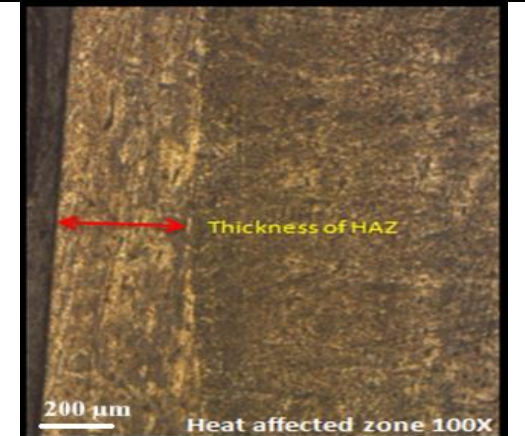The microstructural changes in the HAZ can potentially impact the mechanical properties and performance of the welded joint, making it an important region to consider when evaluating weld quality and integrity. The scale bar at the bottom indicates that the image is at a magnification of 1 mm, allowing for a detailed examination of the microstructural features in the different regions. The metallographic image shows the weld attributes in Figure 6. Welding forms three separate regions in the microstructure of the material. The FZ experiences both melting and solidification, resulting in a cast structure characterized by elongated grains. HAZ
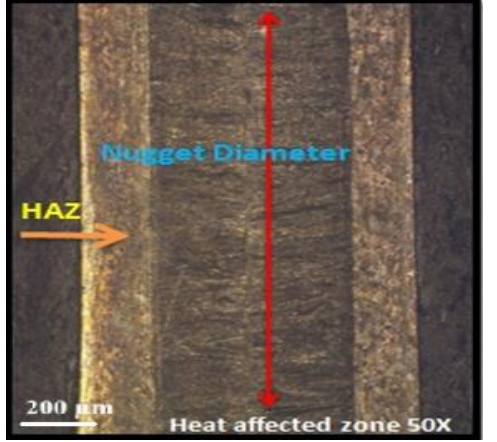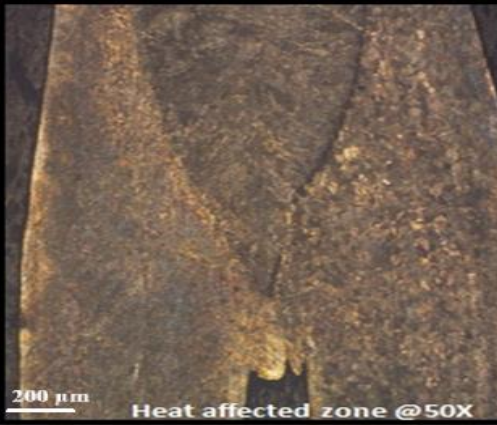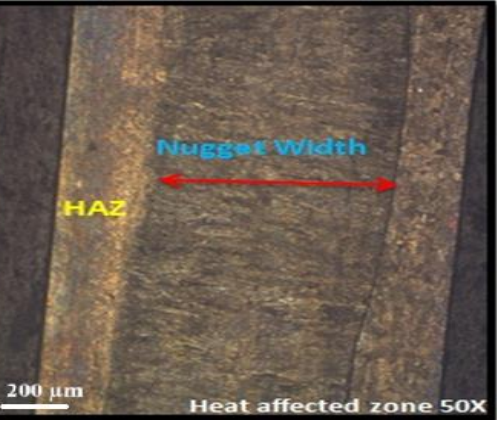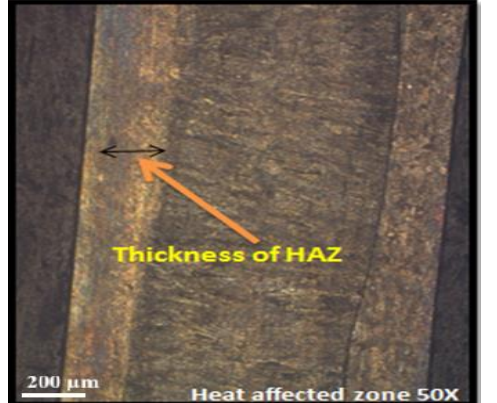
undergoes substantial heat exposure without reaching its melting point, resulting in alterations to its microstructure. The base BM is located farthest from the heat source, therefore maintaining its original microstructure.

The HAZ is the area adjacent to the weld nugget that has experienced elevated temperatures during the welding process, causing microstructural changes but not complete melting. The FZ was observed to exhibit a coarse, dendritic microstructure, typical of cast or rapidly solidified structures in welded materials. The coarse grains and dendritic morphology in this zone indicate that the cooling rate was relatively slow, allowing for significant grain growth and solidification segregation. The HAZ presented a markedly different microstructure compared to both the fusion zone and the base metal. The microstructure in the HAZ was finer and more homogeneous, attributed to the lower peak temperatures and slower thermal cycles experienced in this region. The extent and evolution of the microstructure in the HAZ have a substantial impact on the mechanical properties of the welded joint, including its strength, toughness, and creep resistance. The base metal (BM) showed a typical wrought or recrystallized microstructure, characterized by equiaxed grains and a more uniform distribution of phases or constituents. The distinct microstructural regions observed in the fusion welding process are indicative of localized melting and subsequent solidification.

The coarse dendritic structure in the fusion zone results from high cooling rates and non-equilibrium solidification conditions during welding. Conversely, the finer, more homogeneous microstructure in the HAZ suggests that the thermal cycles were less severe, leading to partial recrystallization or recovery processes. In Figure 7, a distinct boundary between the heat affected zone and the base metal is visible, highlighting the changes in microstructure due to the thermal cycles experienced during welding. The HAZ typically shows a coarser grain structure compared to the base metal, as the high temperatures facilitate grain growth and recrystallization. This can potentially affect the mechanical properties, such as toughness and hardness, within the HAZ region. The image, magnified at 50X, provides a clear view of the microstructural features in the HAZ and its boundary with the unaffected base metal. Understanding the characteristics of the heat affected zone is crucial for evaluating the overall quality and performance of resistance spot welded joints, as the HAZ can be a potential site for failure or degradation in service.

Figure 7: Weld zone for sample 1	Figure 8: Microstructure of base material

Figure 9: Microstructure of weld zone for sample 2	Figure 10: Microstructure of weld zone for sample 3
Figure 11: Microstructure of weld zone for sample 4	Figure 12: Microstructure of weld zone for sample 5
Figure 13: Microstructure of weld zone for sample 6	Figure 14: Microstructure of HAZ for sample 6

Figure 15: Microstructure of weld zone for sample 7	Figure 16: Microstructure of HAZ for sample 7
Figure 17: Microstructure of weld zone for sample 8	Figure 18: Microstructure of HAZ for sample 8
Figure 19: Microstructure of weld zone for sample 9	Figure 20: Microstructure of HAZ for sample 9

4.3 Taguchi analysis

Taguchi method is used for present analysis with the recorded tensile shear strength of each specimen as shown in Table 2. The S/N ratios measures the sensitivity of the quality characteristic, where 'signal' represents the desired effect or mean value, and 'noise' denotes the disruptions caused by external factors. The S/N ratio is computed using $\eta = -10 \log (MSD)$, with MSD being the mean-square deviation of the output. The objective is to maximize the S/N ratio, indicating that the signal significantly surpasses random noise. The S/N ratios for each experiment in the L9 orthogonal array (OA) are summarized in Table 2, with Table 3 showing the response for S/N ratio maximization and Table 4 is the response table for means maximum is the better.

Table 3: Response table for signal to noise ratios

Level	Welding current (A) (kA)	Pressure (B) (Bar)	Weld time (C) (Cycles)
1	45.69	48.02	48.43
2	47.93	47.76	47.45
3	48.63	46.47	46.37
Delta	2.93	1.55	2.06
Rank	1	3	2

Table 4: Response table for means

Level	Welding current (A) (kA)	Pressure (B) (Bar)	Weld time (C) (Cycles)
1	201.1	252.5	264.2
2	249.8	246.8	238.5
3	270.3	221.9	218.5
Delta	69.3	30.5	45.7
Rank	1	3	2

Figure 21 illustrates the main effects plot for means, Figure 22 presents a graph of the signal-to-noise (S/N) ratio with a horizontal line denoting the mean value. A higher S/N ratio signifies improved quality for tensile shear strength. The S/N ratio analysis reveals that the optimal parameter settings for maximizing tensile-shear strength are A3B1C1. The first graph in Figure 22 indicates that increasing the welding current from 6 kA to 10 kA enhances the response variable, likely due to the greater heat input improving fusion and weld penetration. The middle graph shows that the response variable increases as pressure rises from 2 bar to 4 bar but decreases as pressure continues to 6 bar, suggesting an optimal pressure range. Excessive pressure may lead to defects like material expulsion, compromising weld quality. The third graph reveals that as weld time increases from 4 cycles to 8 cycles, the response variable declines, which could be due to excessive heat input causing issues such as melting or porosity. Figure 22's three line graphs demonstrate the relationship between welding current, pressure, and weld time with the S/N ratio. An increase in welding current from 6 kA to 10 kA improves the S/N ratio, indicating better weld quality. Pressure increases the S/N ratio up to 4 bar but decreases beyond this point, suggesting an optimal pressure range. Increasing weld time reduces the S/N ratio, implying shorter weld times are preferable for optimal quality. Thus, the optimal welding settings are higher current, intermediate pressure, and shorter weld time for achieving the best S/N ratio.

Figure 21: Main effects plot for means
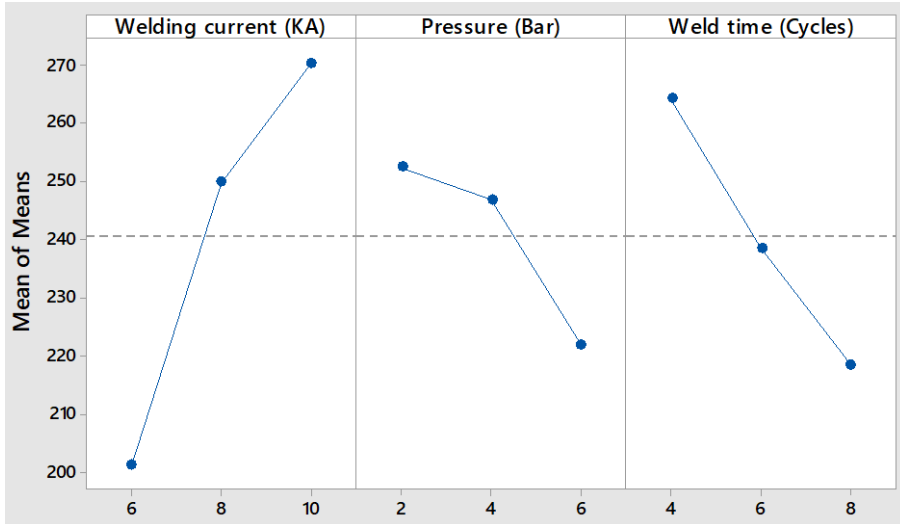
Figure 22: Main effects plot for SN ratios
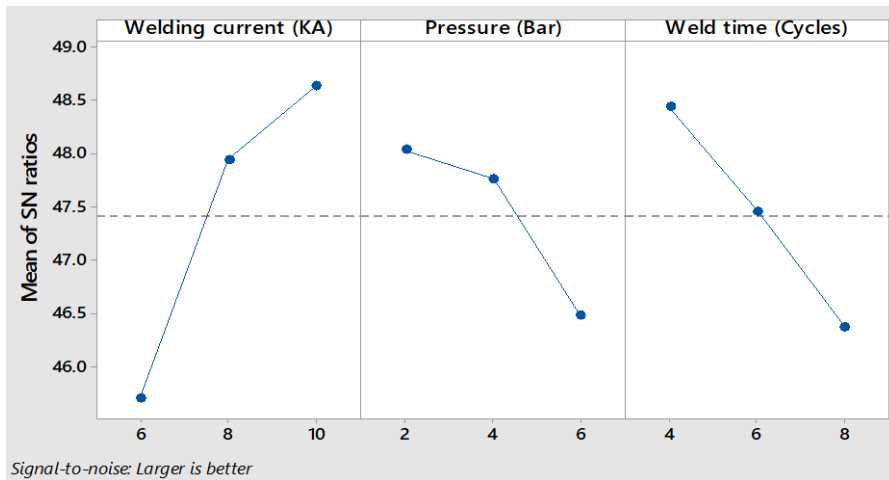
5. Conclusion

In this study, the application of Taguchi method was used to obtain the optimized resistance spot welding parameters for AISI 316L steel grade sheet. The significance of each process parameter is determined by ANOVA. Furthermore, the predicted optimal parameters were used to determine experimental tensile shear strength. The following conclusions were drawn in the present study:

1.   As the welding duration increases, the temperature of the faying surface of the sheets rises rapidly until this area is melted and a nugget is created. Following the creation of the nugget, the pace of temperature increase decreases suddenly. There was no expulsion noted

when the welding time was increased up to 8 cycles, indicating that welding time does not have a substantial impact on expulsion.

2.   Increasing welding time results in higher heat losses from the weld zone, making welding current more effective in enhancing tensile shear strength. Optimize welding current to minimize expulsion, save production time, enhance productivity, and achieve peak tensile shear strength. Taguchi's analysis concluded different optimum values for individual responses. For maximum tensile shear strength, the optimum value for welding current is 10 kA, electrode force is 2 bar, and weld time is 4 cycles/s.

2.   Percentage contribution of welding current was found to be maximum while weld time contributed moderately and pressure had the minimum contribution in the RSW process.

3.   In conclusion, both welding pressure and welding time significantly impact the tensile-shear strength of SS 316L sheet joints. Optimal parameters are current at 10 KA, electrode force is 2 bars and 4 cycle of weld time essential to ensure strong, durable, and reliable welded joints in this material. Balancing these parameters through experimentation and adhering to recommended guidelines can help achieve superior joint strength and overall structural integrity.

Conflict of Interest Statement:

The authors declare that there are no conflicts of interest regarding the publication of this manuscript. We have no financial or personal relationships with individuals or organizations that could influence our work or could be perceived as potential conflicts of interest.

Data Availability Statement:

The data sets generated and/or analyzed during the current study are available from the corresponding author upon reasonable request. Restrictions may apply to the availability of certain data due to privacy or ethical concerns. However, the authors will make every effort to provide access to the data in accordance with applicable regulations and guidelines.

References

1.   De Castro, C. C., Shen, J., Plaine, A. H., Suhuddin, U. F., de Alcântara, N. G., dos Santos, J. F., & Klusemann, B. (2022). Tool wear mechanisms and effects on refill friction stir spot welding of AA2198-T8 sheets. Journal of Materials Research and Technology, 20, 857-866.

2.   Chaudhari, A. Y., & Deshmukh, D. D. (2020, March). Metallurgical investigations on corrosion behavior of simple and heat treated duplex stainless steel 2205 exposed to corrosive media. In IOP Conference Series: Materials Science and Engineering (Vol. 810, No. 1, p. 012048). IOP Publishing.

3.   Xiao, R., Zhao, Y., Liu, H., Oliveira, J. P., Tan, C., Xia, H., & Yang, J. (2022). Dissimilar laser spot welding of aluminum alloy to steel in keyhole mode. Journal of Laser Applications, 34(1).

4.   Baek, S., Song, J., Lee, H. C., Park, S. Y., Song, K. H., Lee, S., ... & Kim, D. (2022). Robust bonding and microstructure behavior of aluminum/high-strength steel lap joints using resistance element welding process for lightweight vehicles: Experimental and numerical investigation. Materials Science and Engineering: A, 833, 142378.

5.   Al-Ani, M. (2023, March). Investigation of mechanical and microstructural characteristics of friction stir spot welded joints of aluminum sheets. In AIP Conference Proceedings (Vol. 2651,

No. 1). AIP Publishing.

6.   Reza Kashyzadeh, K., Farrahi, G. H., Minaei, M., Masajedi, R., Gholamnia, M., & Shademani, M. (2022). Numerical study of shunting effect in three-steel sheets resistance spot welding. International Journal of Engineering, 35(2), 406-416.

7.   Kalyankar, V., Bhoskar, A., Deshmukh, D., & Patil, S. (2022). On the performance of metallurgical behaviour of Stellite 6 cladding deposited on SS316L substrate with PTAW process. Canadian Metallurgical Quarterly, 61(2), 130-144.

8.   Deshmukh, D. D., & Kharche, Y. (2023). Influence of processing conditions on the tensile strength and failure pattern of resistance spot welded SS 316L sheet joint. International Journal on Interactive Design and Manufacturing (IJIDeM), 1-13.

9.   Chen, L., Zhang, Y., Xue, X., Wang, B., Yang, J., Zhang, Z. & Barber, G. C. (2022). Investigation on shearing strength of resistance spot-welded joints of dissimilar steel plates with varying welding current and time. Journal of Materials Research and Technology, 16, 1021-1028.

10.   Rajarajan, C., Sonar, T., Sivaraj, P., Raja, S., & Mathiazhagan, N. (2022). Investigating the effect of electrode pressure on nugget size, microstructure and tensile shear strength of resistance spot welded advanced high strength dual phase steel joints. Metallography, Microstructure, and Analysis, 11(3), 472-483.

11.   Sachin K. Dahake, Nilesh Diwakar, & Shyamkumar D. Kalpande (2023). Optimization of Resistance Spot Welding Parameters for 316L Stainless Steel Using Response Surface Methodology and Box-Behnken Design: Investigation on Joint Characteristics and Performance. Tuijin Jishu/Journal of Propulsion Technology ISSN: 1001-4055 Vol. 44 No. 5. doi: 10.52783/tjjpt.v44.i5.3003.

12.   Ghanbari, H. R., Shariati, M., Sanati, E., & Nejad, R. M. (2022). Effects of spot welded parameters on fatigue behavior of ferrite-martensite dual-phase steel and hybrid joints. Engineering Failure Analysis, 134, 106079.

13.   Betiku, O. T., Ramachandran, D. C., Ghatei-Kalashami, A., DiGiovanni, C., Sherepenko, O., Ghassemi-Armaki, H., & Biro, E. (2023). Improving the mechanical performance of press-hardened steel resistance spot welds via in-situ grain refinement. Journal of Materials Processing Technology, 320, 118122.

14.   Dong, W., Lei, M., Pan, H., Ding, K., & Gao, Y. (2022). Role of the internal oxidation layer in the liquid metal embrittlement during the resistance spot welding of the Zn-coated advanced high strength steel. Journal of Materials Research and Technology, 21, 3313-3326.

15.   Wippermann, J., Meschut, G., Koshukow, W., Liebsch, A., Gude, M., Minch, S., & Kolbe, B. (2023). Thermal influence of resistance spot welding on a nearby overmolded thermoplastic–metal joint. Welding in the World, 67(3), 793-804.

16.   Zhao, D., Vdonin, N., Radionova, L., Glebov, L., & Bykov, V. (2022). Optimization of post-weld tempering parameters for HSLA 420 steel in resistance spot welding process. The International Journal of Advanced Manufacturing Technology, 123(5-6), 1811-1823.

17.   Aswar S. J., Diwakar Nilesh & Kalpande S. D. (2023). Investigations And Optimization Of Laser Process Parameters Using Box Benhken Design Approach For Advanced Materials. Journal of Aeronautical Materials Vol. 43, Issue-01, 2023 pp. 525-542.

18.   Kakade, S., Thakur, A., Patil, S., & Deshmukh, D. (2023). Experimental evaluation and correlation of plasma transferred arc welding parameters with hardfacing defects. In Recent Advances in Material, Manufacturing, and Machine Learning (pp. 326-331). CRC Press.

19.   Guo, J., Bi, J., Wang, S., Li, Y., Manladan, S. M., & Luo, Z. (2022). Modeling the effect of electrode morphology on Mg/steel resistance spot welding. The International Journal of Advanced Manufacturing Technology, 120(1-2), 137-148.

20.   Yaghoobi, F., Jamaati, R., & Aval, H. J. (2022). Resistance spot welding of high-strength DP steel and nano/ultrafine-grained IF steel sheets. Materials Chemistry and Physics, 281, 125909.

21.   Kakade, S. P., Thakur, A. G., Deshmukh, D. D., & Patil, S. B. (2022). Experimental investigations and optimisation of Ni-Cr-B-Si hardfacing characteristics deposited by PTAW process on SS 410 using response surface method. Advances in Materials and Processing Technologies, 1-17.

22.   Chaudhari A. Y., Diwakar Nilesh & Kalpande S. D. (2023). Mechanical characteristics, morphology and corrosion behavior of duplex stainless steel 2205. Eur. Chem. Bull. 2023,12(Special issue 8), 4900-4910.

23.   Naik, H. V., Deshmukh, D. D., & Kalyankar, V. D. (2019). Study of heat treatment effect on microstructure of PTA weld deposited surface of SS 316L steel. In Advances in Additive Manufacturing and Joining: Proceedings of AIMTDR 2018 (pp. 597-607). Singapore: Springer Singapore.

24.   Kalyankar, V. D., & Deshmukh, D. D. (2017, December). Failure investigations of failed valve plug SS410 steel due to cracking. In IOP Conference Series: Materials Science and Engineering (Vol. 282, No. 1, p. 012007). IOP Publishing.

25.   Deshmukh, D. D., & Kalyankar, V. D. (2019). Deposition Characteristics of Multitrack Overlay by Plasma Transferred Arc Welding on SS316Lwith Co-Cr Based Alloy–Influence ofProcess Parameters. High Temperature Materials and Processes, 38(2019), 248-263.

26.   Deshmukh, D. D., & Kalyankar, V. D. (2018). Recent status of overlay by plasma transferred arc welding technique. International Journal of Materials and Product Technology, 56(1-2), 23-83.

27.   Deshmukh, D. D., & Kalyankar, V. D. (2019). Evaluation of surface characteristics of PTAW hardfacing based on energy and powder supplied. In Advances in Micro and Nano Manufacturing and Surface Engineering: Proceedings of AIMTDR 2018 (pp. 547-558). Singapore: Springer Singapore.

28.   Ding, K., Dong, W., Lei, M., Wang, L., Pan, H., & Gao, Y. (2022). Oxidation-assisted crack propagation of the liquid metal embrittlement in the resistance spot welded steels. Materials Characterization, 194, 112438.

29.   Manladan, S. M., Jang, Y., & Park, Y. D. (2023). Effect of paint baking on the halo ring and mechanical behavior of 30MnB5 hot-stamped steel resistance spot welding joints. Journal of Materials Research and Technology, 24, 4756-4761.

30.   Yang, Y., Li, Y., Bi, J., Liu, H., Ao, S., & Luo, Z. (2022). Microstructure and mechanical properties of 2195/5A06 dissimilar joints made by resistance spot welding. Materials Characterization, 191, 112147.

31.   Pestka, J., & Weihe, S. (2022, November). Influence of the Joining Force on the Nugget Diameter During Resistance Spot Welding of Aluminum Materials. In Stuttgart Conference on Automotive Production (pp. 96-107). Cham: Springer International Publishing.

32.   Kumar, N., Ramakrishnan, S. M., Panchapakesan, K., Subramaniam, D., Masters, I., Dowson, M., & Das, A. (2022). In-depth evaluation of micro-resistance spot welding for connecting tab to 18,650 Li-ion cells for electric vehicle battery application. The International Journal of Advanced Manufacturing Technology, 121(9-10), 6581-6597.

33.   Sharma, S. K., Patel, P., Chandra, M., Rajak, A. K., & Sharma, C. (2022). Resistance Spot Welding of Aluminum 6063 Alloy for Aerospace Application: Improvement of Microstructural and Mechanical Properties. Journal of The Institution of Engineers (India): Series D, 103(1), 311-318.

34.   Bhoskar, A., Kalyankar, V., & Deshmukh, D. (2023). Metallurgical characterisation of multi-track Stellite 6 coating on SS316L substrate. Canadian Metallurgical Quarterly, 62(4), 665-677.

35.   Hamidinejad, S., Kolahan, F., & Kokabi, A. (2012). The modelling and process analysis of resistance spot welding on galvanized steel sheets used in car body manufacturing. Materials & Design, 34, 759-767. doi: 10.1016/j.matdes.2011.06.064.